

Accepted Manuscript

Bone-targeting nanoparticle to co-deliver decitabine and arsenic trioxide for effective therapy of myelodysplastic syndrome with low systemic toxicity

Xiaoyan Wu, Zhenhua Hu, Sara Nizzero, Guodong Zhang, R. Maricela Ramirez, Ce Shi, Jin Zhou, Mauro Ferrari, Haifa Shen



PII: S0168-3659(17)30901-X
DOI: doi:[10.1016/j.jconrel.2017.10.012](https://doi.org/10.1016/j.jconrel.2017.10.012)
Reference: COREL 8999

To appear in: *Journal of Controlled Release*

Received date: 30 May 2017
Revised date: 23 September 2017
Accepted date: 12 October 2017

Please cite this article as: Xiaoyan Wu, Zhenhua Hu, Sara Nizzero, Guodong Zhang, R. Maricela Ramirez, Ce Shi, Jin Zhou, Mauro Ferrari, Haifa Shen , Bone-targeting nanoparticle to co-deliver decitabine and arsenic trioxide for effective therapy of myelodysplastic syndrome with low systemic toxicity. The address for the corresponding author was captured as affiliation for all authors. Please check if appropriate. Corel(2017), doi:[10.1016/j.jconrel.2017.10.012](https://doi.org/10.1016/j.jconrel.2017.10.012)

This is a PDF file of an unedited manuscript that has been accepted for publication. As a service to our customers we are providing this early version of the manuscript. The manuscript will undergo copyediting, typesetting, and review of the resulting proof before it is published in its final form. Please note that during the production process errors may be discovered which could affect the content, and all legal disclaimers that apply to the journal pertain.

Bone-targeting nanoparticle to co-deliver decitabine and arsenic trioxide for effective therapy of myelodysplastic syndrome with low systemic toxicity

Xiaoyan Wu^{a,b,*}, Zhenhua Hu^{a*}, Sara Nizzero^a, Guodong Zhang^a, Maricela Ramirez R^a, Ce Shi^c, Jin Zhou^c, Mauro Ferrari^{a,d}, Haifa Shen^{a,e}

Affiliations:

^aDepartment of Nanomedicine, Houston Methodist Research Institute, Houston, Texas 77030, USA.

^bDepartment of Pediatric Hematology, Union Hospital, Tongji Medical College, Huazhong University of Science and Technology, Wuhan, China 430022.

^cDepartment of Hematology, First Affiliated Hospital, Harbin Medical University, Harbin, China 150081.

^dDepartment of Medicine, Weill Cornell Medical College, New York, New York, USA.

^eDepartment of Cell and Developmental Biology, Weill Cornell Medical College, New York, New York 10065, USA.

* Xiaoyan Wu and Zhenhua Hu contributed equally to this article

Corresponding author:

Haifa Shen, MD, Ph.D., Department of Nanomedicine, Houston Methodist Research Institute, 6670 Bertner Avenue, Houston, Texas 77030

hshen@houstonmethodist.org

Keywords:

Myelodysplastic syndrome, bone marrow, delivery, nanoparticle, decitabine, arsenic trioxide

Abstract

Myelodysplastic syndromes (MDS) are a diverse group of bone marrow disorders and clonal hematopoietic stem cell disorders characterized by abnormal blood cells, or reduced peripheral blood cell count. Recent clinical studies on combination therapy of decitabine (DAC) and arsenic trioxide (ATO) have demonstrated synergy on MDS treatment, but the treatment can cause significant side effects to patients. In addition, both drugs have to be administered on a daily basis due to their short half-lives. In addressing key issues of reducing toxic side effects and improving pharmacokinetic profiles of the therapeutic agents, we have developed a new formulation by co-packaging DAC and ATO into alendronate-conjugated bone-targeting nanoparticles (BTNPs). Our pharmacokinetic studies revealed that intravenously administered BTNPs increased circulation time up to 3 days. Biodistribution analysis showed that the BTNP facilitated DAC and ATO accumulation in the bone, which is 6.7 and 7.9 times more than untargeted NP. Finally, MDS mouse model treated with BTNPs showed better restoration of complete blood count to normal level, and significantly longer median survival as compared to free drugs or untargeted NPs treatment. Our results support bone-targeted co-delivery of DAC and ATO for effective treatment of MDS.

1. Introduction

Myelodysplastic syndromes (MDS) are a diverse group of bone marrow disorders or clonal hematopoietic stem cell disorders characterized by abnormal blood cells (dysplasia), or reduced peripheral blood cell count (cytopenia), and has the risk of transformation to acute myeloid leukemia, primarily in the elderly population. Morbidity and mortality in MDS are mostly caused by cytopenia and transformation to leukemia [1]. Currently, the goal of MDS treatment is to achieve hematologic improvement and alteration of the natural progression of the disease [2]. Despite variety of treatments developed in the past years, the use of a single therapeutic agent remains limited by the biological heterogeneity of MDS and its complex mechanism [3, 4]. Instead, combination therapies using multiple therapeutic agents have been proposed to eradicate MDS cells by exploiting synergistic effects among drugs, and to reduce adverse effects. It was shown in a recent trial that the combination of decitabine (DAC) and arsenic trioxide (ATO) almost tripled the response rate in MDS patients compared to single agent therapies [5-7]. The synergistic effect was reflected by the dual-action of inhibition of methylation and induction of leukemia stem cell apoptosis [8]. However, systemic toxicity from DAC and ATO is a major cause for concern. For example, daily and continued administration of ATO for single agent treatment of MDS has been reported to cause lethal hepatic damage in clinic [9, 10]. Some studies have shown that nonspecific global demethylation generated by DAC may lead to global chromosomal instability and contribute to neoplasm [11, 12]. Moreover, because of the short half-lives of both DAC and ATO, daily administration is necessary to sustain therapeutic effect. The continuous injections of these two drugs have several drawbacks such as increased cost and poor patient compliance. These problems highlight the urgent need in targeting these two drugs in disease tissue to

reduce systemic toxicity and to sustainably release these drugs over time so as to improve patient compliance.

Nanomedicine has been addressing toxicity and delivery issues of systemically administered drug for several decades now [13]. In this field, various nanoformulations have been explored to co-deliver therapeutic agents to treat different diseases. Examples include nanoscale polymer particles for co-delivery of oxaliplatin and gemcitabine [14], carboxymethyl chitosan micelle for doxorubicin and cisplatin [15], liposomes for oxaliplatin and cetuximab [16], mesoporous silica nanoparticles for cisplatin and phthalocyanine [17], pH sensitive hydrogel for paclitaxel and doxorubicin [18]. Up to now, there has been no nanomedicine reported to successfully co-deliver drugs for treatment of MDS. However, there are two types of nanoparticles loaded with single drugs reported to treat MDS: magnetic nanoparticle (MNPs-Fe₃O₄), and PLA-PEG polymeric nanoparticle. The efficacy of MNPs-Fe₃O₄ was only evaluated on MDS cells [19]. On the other hand, PLA-PEG nanoparticle loaded with AZD2811, termed Accurins, is currently in clinical trial stage. Although Accurins has improved toxicity and antitumor activity through slow release kinetics of PLA-PEG polymer nanoparticles, its non-specific distribution and release still result in significant systemic toxicity [20]. Thus, to maximally enhance therapy efficacy and reduce systemic toxicity of chemotherapy drugs, effective targeted delivery of drug molecules to the bone marrow where MDS cells reside is still an urgent need. Alendronate (ALN), a bisphosphonate, has emerged in recent years as a highly effective bone or bone microenvironment targeting ligand thanks to its strong chelation with the calcium ion of mineral hydroxyapatite (HA), the main ingredient of bone marrow niches [21]. Different bone targeted delivery systems based on bisphosphonates, especially alendronate, have been developed for the treatment of bone-related cancers. These systems

mainly include polymeric (PTX-PEG-ALN, DOX-hyd-PEG-ALN) [22, 23] and liposomal (LIP-ALN) nanoparticles [24]. However, these two kinds of bone-targeted nanoparticles have their intrinsic drawbacks. In fact, liposomes lack stability, high drug loading, and sustained-release properties, whereas polymeric nanoparticles aggregate easily due to their hydrophobic surface [25]. In this work we developed alendronate-conjugated bone-targeting nanoparticles (BTNPs) to co-deliver DAC and ATO to bone marrow for treatment of MDS. The core of BTNPs consists of a poly (D, L-lactide-co-glycolide)-cholesterol polymer that releases the drugs in a controlled fashion, and the shell is made of alendronate-PEG-lipid designed to target bone marrow. BTNPs combine the advantages of both polymeric nanoparticles and liposomes to obtain efficient drug encapsulation, time-tunable drug release profile, and bone marrow targeting potential [25-27]. In addition, all components of BTNPs are biodegradable, biocompatible, and FDA-approved, thus making BTNPs suitable for clinical translation. Overall, the purpose of BTNPs is to co-deliver of DAC and ATO and increase enrichment of the drugs in bone marrow microenvironment, which may enhance synergistic treatment of MDS and reduce systemic toxicity of chemotherapeutics.

2. Materials and methods

2.1. Materials

DAC and ATO were purchased from LC laboratories (Boston, MS, USA). RPMI 1640 and fetal bovine serum (FBS) were obtained from Thermo Fisher (Waltham, MA, USA). FITC-AnnexinV and 7-AAD were ordered from Invitrogen (Carlsbad, CA, USA). poly (D, L-lactide-co-glycolide)-cholesterol (5050) (inherent viscosity: 0.59 dL/g, average Mn: 38 kDa) was purchased from PolySciTech (West Lafayette, USA). Alendronate sodium trihydrate, polyvinyl alcohol and primer were ordered from Sigma-Aldrich (St. Louis, MO, USA). 1, 2-Distearoyl-sn-glycero-3-

phosphoethanolamine-N-[carboxy (polyethylene glycol)-2000] was purchased from Avanti Polar Lipids, Inc. (Alabaster, AL, USA).

2.2. Bone marrow cell isolation and culture

Bone marrow cells were extracted from the femur and tibia of wild-type and MDS-bearing mice by flushing the bone marrow cavity with 2% FBS in PBS using 25G needles. Collected cells were centrifuged at 1,500 rpm for 3.5 min and then resuspended in the ammonium-chloride-potassium lysis buffer for 20 sec to lyse red blood cells. Cells were then centrifuged at 1,500 rpm for 3.5 min, resuspended in 2% FBS, and then filtrated using a sterile cell strainer with 70 μ m nylon mesh. The collected bone marrow cells were cultured in RPMI 1640 medium enriched with m-IL-6, m-IL-3 and m-SCF in a 37°C incubator. Smears of a portion of the collected fresh bone marrow cells were also stained by the Wright-Giemsa method.

2.3. Preparation of Alendronate-PEG-DSPE

25 mg of 1,2-distearoyl-sn-glycero-3-phosphoethanolamine-N-[carboxy(Poly ethylene glycol)-2000] (DSPE-PEG-COOH) were dissolved in acetone and methanol (about 10 mg/mL), and then the solution was added drop by drop into ten times volume of phosphate buffer (50 mM, pH 7.2), and left stirring for 4 hour at room temperature. The lipid micelle solution was concentrated to 1 mL and transferred to 1.5 mL tube. Ethyl-3-(3-dimethylaminopropyl) carbodiimide (EDC) and N-hydroxysuccinimide (NHS) (both 2 equivalent of Carboxylic acid groups) were added to the lipid micelle solution, and stirred for 1 hour at room temperature. The lipid micelle solution was diluted adding 4 mL Mill-Q water, and then excess EDC and NHS from the diluted solution were removed using 3KDa ultra-centrifuge filters. 20 mg of Alendronate were dissolved in 1 mL sodium borate

buffer (pH 8.5, 100 mM), then added to the concentrated lipid micelle solution and stirred overnight at room temperature. Alendronate conjugated lipid was transferred to 2000 MWCO benzoylated cellulose dialysis bag and dialyzed against water for 24 hours at room temperature. The water was changed for 4 times. The dialyzed conjugated lipid was lyophilized, yielding to about 21.0 mg of white powder. The dried conjugated lipid powder was dissolved in acetone, then flushed with nitrogen to dry, and stored at 4°C until use.

2.4. Preparation of DAC and ATO encapsulated BTNPs

100 µl of ATO and DAC dissolved in NaOH (3 mg/ml) was added into a solution of 50 mg poly (D, L-lactide-co-glycolide)-cholesterol dissolved in 1 ml dichloromethane under vortex to form a W/O primary emulsion. The primary emulsion was added into 1.6 ml of 5% polyvinyl alcohol and 2 mg/ml of alendronate-poly (ethylene glycol)-1, 2-distearoylsn-glycero-3-phosphoethanolamine (Alendronate-PEG-DSPE). The resulting emulsion was then sonicated three times for 30 s at 70 Hz. The mixture was then added to 100 ml of 0.2% polyvinyl alcohol, and left stirring for 3 h to remove the organic solvent. Particles were washed by centrifugation at 10,000 rpm for 20 min at 4°C, and then washed three times with deionized water. The collected particles were lyophilized and stored at –20°C [28]. BTNPs loaded with only DAC or ATO were prepared as control following the same process. Untargeted nanoparticles (Untargeted NPs) were prepared by the same process using DSPE-PEG-COOH.

2.5 Characterization of BTNPs

2.5.1 Particle size and surface charge

To measure particle size, empty BTNPs were dispersed homogeneously in deionized water at 2 mg/ml by ultrasonication. Size and zeta potential of BTNPs were measured using a Zetasizer Nano ZS90 (Malvern Instruments, Malvern, UK) following the manufacturer recommended protocols. All measurements were confirmed by triplicates, and results refer to the mean of three measurements/one of the triplicates is shown. Topographical images of BTNPs using atomic force microscopy (AFM) imaging in air was performed on a dry sample of NP deposited on a silicon slide to confirm particles' morphology. Particles were imaged using a commercial silicon cantilever in tapping mode at a scanning rate of 0.5 Hz from a 0° angle. Images were processed by fitting each scan line to polynomial leveling functions [29].

2.5.2 Structure analysis of BTNPs

A negative stain was used to examine the lipid layer on surface of BTNPs with transmission electron microscopy (TEM), following a previously reported procedure [30]. Briefly, BTNPs were diluted in deionized water at 2 mg/ml and sonicated. Samples were then prepared by placing one drop of 10 times diluted BTNPs on a carbon-coated copper grid. After air dry for 10 minutes on the grid, particles were stained with 2% phosphotungstic acid for 15 minutes. The stained samples were imaged using a TEM (3H-7000FA; Hitachi Ltd.). Scanning electron microscopy (SEM) was used to observe the solid core of polymer structure. The BTNPs dispersed in deionized water at 2 mg/ml were dropped onto a silica slide and allowed to dry. To enhance conductivity, a 5 nm thick gold layer was deposited onto the sample before imaging.

2.6 Measurement of drug loading and encapsulation efficiency in BTNPs

Five formulations of BTNPs including different ratio of DAC/ATO (w/w) was performed listed in Table S1: BTNPs (0:1), BTNPs (0.5:1), BTNPs (1:1), BTNPs (2:1) and BTNPs (3:1). The amount of DAC in BTNPs was measured using high performance liquid chromatography (HPLC) following a procedure previously published [31]. Briefly, dried BTNPs were dissolved into dimethyl sulfoxide under vortex for 60 sec, and centrifuged at 10,000 rpm for 10 min. The supernatant was collected and applied for HPLC separation. The mobile phase was 0.14 M acetic acid and acetonitrile, and gradient elution (starting at 10% acetonitrile and ending at 90% acetonitrile after 20 minutes) was used to separate DAC. DAC was detected at a wavelength of 230 nm. The retention time of DAC was 9.7min. The standard curve was obtained in the range between 5–500 ng/mL with regression equation $Y = 125.23X - 147.568$ and correlation coefficient $R^2 = 0.9994$. The amount of ATO in BTNPs was determined using an inductively coupled plasma (ICP) method, as previously described [32, 33]. To prepare samples, dried nanoparticles were dissolved in methanol and acetonitrile (3:1), and centrifuged at 12,000 rpm for 10 min. The supernatant was carefully removed, and the precipitate was dissolved in 0.1 M NaOH and used for ICP analysis. The drug loading (DL) and encapsulation efficiency (EE) were calculated as $DL = (W_1/W) \times 100\%$, and $EE = (W_1/W_2) \times 100\%$, where W_1 is the mass of drug loaded in nanoparticles, W_2 is the initial amount of drug added in solution for the loading, and W is the mass of nanoparticles.

2.7 *In vitro* drug release from BTNPs

In vitro drug release profiles were performed in PBS, pH 7.4. Briefly, 10 mg of BTNPs were dispersed into 2 ml PBS and incubated in air at 37°C with shaking at 500 rpm. After centrifugation at 12,000 rpm, 4°C for 10 min, the supernatant was collected and analyzed following the method for drug loading at interval time. 2 mL of fresh PBS solution was added to the tube for the next readings. A time-dependent accumulative release curve was generated by repeating this at different times.

2.8 Cytotoxicity of BTNPs

Cytotoxicity of BTNPs (DAC: ATO) in MDS and WT bone marrow cells was evaluated through MTT assay. Briefly, cells were seeded into 96-well plates at a seeding density of 1×10^5 cells/well, and treated with increasing concentrations of five different formulations of BTNPs (ATO only, 0.5:1, 1:1, 2:1, 3:1) at different equivalent concentrations of ATO (0.001, 0.01, 0.1, 1, 10, 50, and 100 $\mu\text{g/mL}$) in triplicates. Based on the ratio of DAC/ATO in each formulation, the corresponding DAC concentrations can be calculated for each formulation. Cells were cultured for 72 h before evaluated for cell viability. To measure cell viability, 10 μl of MTT reagent was added to each well and incubated at 37°C for 4 h before dimethyl sulfoxide was added into each well. Optical density (OD) values were measured at 590 nm using a microplate reader. Percentage of cell survival was calculated using untreated cells as the control. Synergistic inhibition effect was defined as $\text{CI} < 1$.

2.9 Apoptosis analysis of bone marrow cells

Apoptosis was analyzed with annexin V-fluorescein isothiocyanate (FITC)/7-AAD double staining following a previously published procedure [34]. Briefly, MDS mouse bone marrow cells (1×10^5 cells/mL) were seeded in 6 well plates and treated with free DAC+ATO, DAC/ATO untargeted NPs, and DAC/ATO BTNPs with an equivalent concentration of ATO of 0.1 $\mu\text{g/mL}$ for 24 h. Then, cells were stained with Annexin V-FITC/7-AAD dye according to the manufacturer's instructions. Cells treated with PBS were used as control. Finally, cells were harvested and used for flow cytometry, H&E staining or fluorescence microscopy.

2.10 *In-vitro* colloidal stability of BTNPs

BTNPs were dispersed in 50% fetal bovine serum (FBS, GenDEPOT, TX, USA) solution at 2 mg/mL. At each time point, an aliquot of BTNPs solution was collected to measure BTNPs size using the same method described in 2.5.1.

2.11 Pharmacokinetics studies

Untargeted nanoparticles and BTNPs were injected into MDS mice via intravenous injection at doses of 6.6 mg/kg DAC and 3.3 mg/kg of ATO. Blood samples were collected into EDTA-K tube by retro-orbital bleeding at scheduled time points. Plasma was separated by centrifuging at 4°C at 3,000 g for 15 min. Each plasma sample was divided into two parts, one for DAC measurement and the other for ATO measurement, respectively. Briefly, 200 µl plasma was mixed with a solution of chloroform and methanol (1:3, v/v) under vortex for 120 s. The mixture was then centrifuged at 12,000 g for 10 min. The organic layer was collected and dried under vacuum following a previously published procedure [35], and then dissolved in 50 µL 0.1 M NaOH. Concentration of DAC in this aliquot was measured by HPLC as described in section 2.5. ATO concentration in the other aliquot was directly diluted with deionized water and used to analyze ATO by ICP as described in 2.5.

2.12 Bone targeting ability of BTNPs

The bone targeting ability of BTNPs was investigated in MDS mice. Alexa 647-labeled lipids were encapsulated into BTNPs to track distribution of nanoparticle *in vivo*. 24 h prior to imaging, 1 mg of Alexa 647-labeled lipid-polymer nanoparticles dispersed in phosphate buffer saline (PBS) was injected intravenously. Whole body fluorescence images were taken with an *in vivo* imaging system (IVIS). Mice injected with fluorescent dye Alexa 647, untargeted particles were used as a

control for bone targeting ability. Mice injected with PBS were used to evaluate background fluorescence. Each mouse had more than 30 point source selections. Quantitative imaging analysis of fluorescence was performed using Living Image Software 4.2 (Caliper Life Sciences, Hopkinton USA).

2.13 Tissue biodistribution analysis

For tissue distribution study, MDS mice were sacrificed at 24 h after treatment with 6.6 mg/kg DAC and 3.3 mg/kg ATO. Tissues were collected and homogenized in PBS followed by the addition of a fourfold volume of extraction solution of chloroform and methanol (1/3, v/v). The mixture was vortexed for 30 min and then centrifuged at 12,000 rpm for 15 min. Each organ processed as described was then separated into two parts [36, 37]. One part was processed for HPLC analysis of DAC content following the procedure described in Section 2.5. The dried organic layer was dissolved in 200 μ L 0.1M NaOH and analyzed using HPLC as described above. The other aliquot was used for ICP analysis of ATO as described above. Femur bone samples were incubated in 14M HNO₃ at 110°C until dried. And then one parts of the powder was dissolved into 0.1 M NaOH for analysis of DAC. The other parts were dissolved into 0.05 M HNO₃ for analysis of ATO. DAC and ATO were then analyzed using HPLC and ICP as described in section 2.5, respectively.

2.14 Therapeutic efficacy studies

All animal studies described above were in accordance with guidelines determined by the Animal Welfare Act and the Guide for the Care and Use of Laboratory Animals, and complied with protocols approved by the Institutional Animal Care and Use Committee (IACUC) at the Houston Methodist Research Institute.

NUP98/HOXD13 transgenic mice [C57BL/6-Tg (Vav1-NUP98/HOXD13) G2Apl/J, Jackson Laboratory] were used as animal model to develop MDS upon aging. To evaluate the efficacy of BTNPs *in vivo*, MDS mice (n=16 mice) were treated with 1) PBS, 2) a solution of free DAC and ATO, 3) untargeted DAC/ATO-NPs, or 4) BTNPs for 4 weeks. PBS and free drug groups were administered daily. NPs and BTNPs groups were administered twice per week. Each group was treated with doses of 6.6 mg/kg DAC and 3.3 mg/kg ATO at each time point. Complete blood count (CBC) was monitored weekly during treatment. Smears of peripheral blood were also stained by the Wright-Giemsa method.

2.15 Real-time RT-PCR analysis

Total RNA was isolated from MDS bone marrow cells using RNeasy Mini kits was used to synthesize cDNA. cDNA and DNMT1 primer were mixed with Premix Ex Taq for real-time PCR analysis. Real-time PCRs data were processed on an Mx3000 multiplex quantitative PCR system. The DNMT1 primers used for real-time PCR analysis were 5'-CCTAGTTCCGTGGCTACGAGGAGAA and 5'-TCTCTCTCC TCTGCAGC CGACTCA.

2.16 Statistical analysis

All data's error bars are reflected as the mean \pm SEM. The 2-tailed Student's t test was applied to compute P values between two groups. Log-rank analyses were used to analyze significance in Kaplan-Meier survival curves. GraphPad Prism software was used to carry out all statistical analyses. *p < 0.05, **p < 0.01, ***p < 0.001. Combination index (CI) was calculated based on cell viability data using the CompuSyn software.

3. Results

3.1 Characterization and biodistribution of bone marrow-targeted BTNPs

We designed a core-shell structure for the BTNP to specifically deliver drug molecules to the bone marrow niches where MDS originates (Fig. 1a). The shell of BTNP was composed of alendronate-conjugated PEG-DSPE for bone targeting, and the PLGA-cholesterol core incorporated DCA and ATO together. The core-shell structure and overall morphology of BTNP were confirmed by SEM, TEM, and AFM, respectively (Fig. 1b-d). The solid core of BTNPs can be seen in the SEM image. The negative staining TEM image showed the lipid shell on the surface of BTNPs. AFM image showed the 3D overall morphology of BTNP. Changes in the lipid-to-polymer ratio resulted in alterations in particle size and surface charge (Fig. 1e). However, alterations in drug composition or ratio did not significantly change particle size (Table S1). DAC and ATO were co-encapsulated into BTNPs with high encapsulation efficiency from 79.2% to 87.5%. BTNPs-ATO had the highest total drug loading and encapsulation efficiency: 4.38% and 87.5%. This is likely due to the faster diffusion of DAC from the BTNP embryo emulsion compared to ATO, which causes more drug leakage during the encapsulation process. The faster diffusion from BTNPs could also be seen from the higher *in vitro* release rate of DAC compared to ATO. The *in vitro* release of DAC and ATO from BNTPs showed that the initial release of both drugs increased with increased content of DAC in BNTPs. Over 72 hours, BTNPs (3:1) and BTNPs (2:1) achieved release of more than 80% of the total drug loaded (Fig. S1). The stable size of BTNPs in 50% FBS solution suggested the good stability of BTNPs and no aggregation in the presence of serum (Fig. S2). Bone targeting ability of BTNPs was confirmed in the *in vivo* biodistribution study where fluorescently labeled BTNPs were used to treat mice with MDS (NUP98/HOXD13 transgenic

mice). Mice administered with BTNPs showed increased retention in all bone tissues (femur, spine, and skull) 24 h later when compared to those treated with untargeted NPs (Fig. 1f, h-j), whereas the florescent dye was mainly retained in kidneys and spleen 24 h after administration (Fig. 1g).

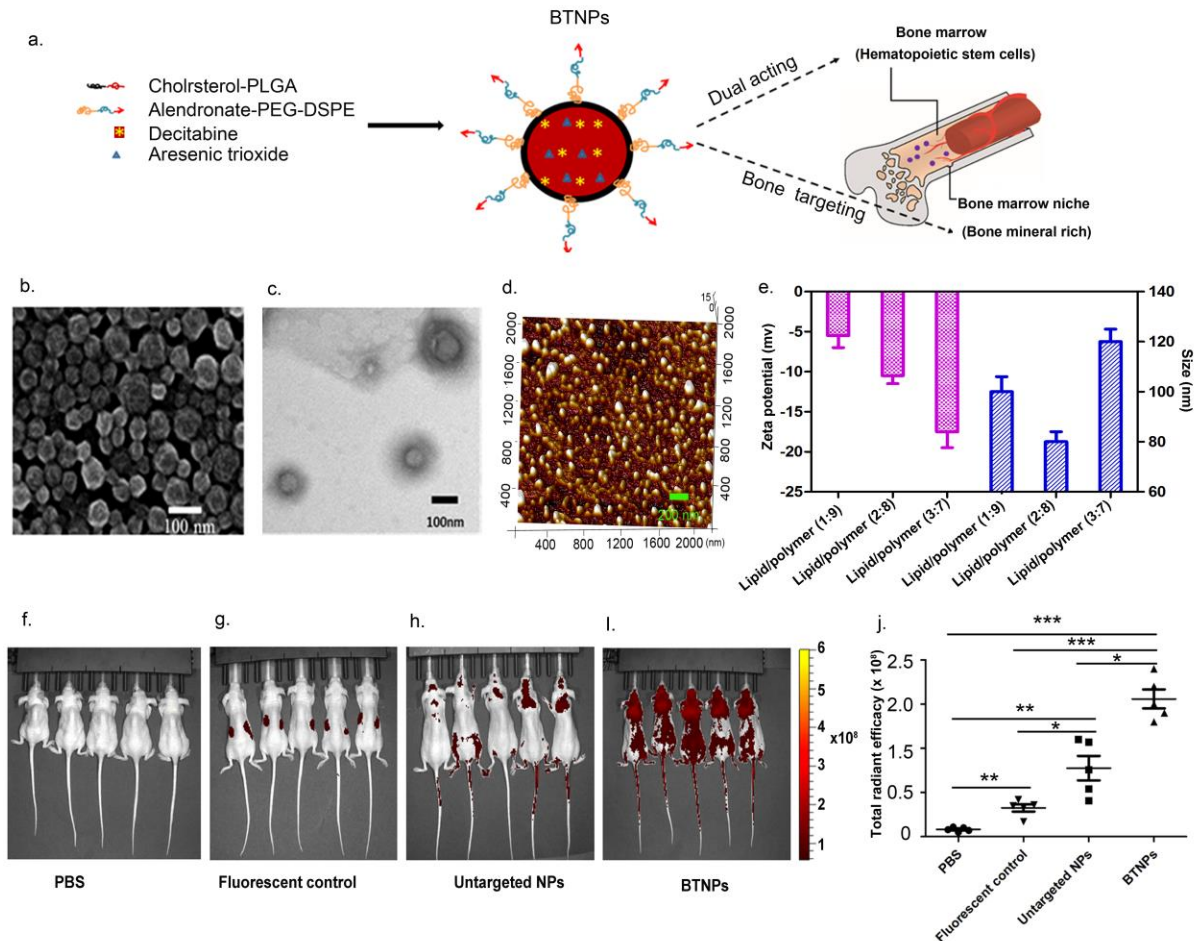


Fig.1. Design, preparation and characterization of bone-targeting nanoparticles (BTNPs). a, Schematic illustration of designed structure of BTNPs. b-d, Representative SEM, TEM and AFM image of BTNPs. e, Physicochemical characteristics of BTNPs. f-i, IVIS of whole-body mice to show BTNPs distribution compared with untargeted NPs, fluorescent control, and PBS (24-h time point, I.V. injection). j, Total fluorescence quantified in the region of interest of IVIS images from f-i.

3.2 Synergistic inhibition of MDS cell growth by BTNP-packaged DAC and ATO

MDS and wild-type bone marrow cells were treated with BTNP-packaged DAC and ATO, and cell viability was examined. In general, we observed an ATO-concentration dependent cell killing, and inclusion of DAC in the formulations enhanced the cytotoxic effect (Fig. 2a). On the contrary, DAC alone at low concentration (0.01 to 1 $\mu\text{g/mL}$) and blank NPs resulted in almost no growth inhibition effects on MDS cells (Fig. S3). All three formulations with DAC: ATO ratios within 1:1 to 3:1 showed synergistic MDS cell killing, as the combination index (CI) was well below 1 (Fig. 2b). Differential cell killing between MDS and wild-type bone marrow cells was observed within 0.01 to 0.5 equivalent ATO concentration range for these three formulations. When treated with the BTNP (2:1) formulation containing DAC/ATO at a 2/1 ratio, viability of MDS cells stayed at 63%, 43%, and 33% at 0.01, 0.1, and 0.5 $\mu\text{g/mL}$ equivalent ATO concentration, respectively; in comparison, viability of wild-type bone marrow cells stayed at 89%, 70%, and 63% when treated with the same dosages (Fig. 2c). In addition, formulation into nanoparticles enhanced MDS cell killing, especially at the 0.01 to 0.5 equivalent ATO concentration range (Fig. 2d). Ideally, BTNPs should have high cell growth inhibition on MDS cells and low cell cytotoxicity on WT cells. Among all the different formulations, only BTNPs (1:1) and BTNPs (2:1) showed the lowest cytotoxicity in WT cells and high synergistic effect in MDS cells. However, *In vitro* release studies showed that BTNPs (1:1) could not achieve complete release of both drugs. Therefore, BTNPs (2:1) was selected for further studies.

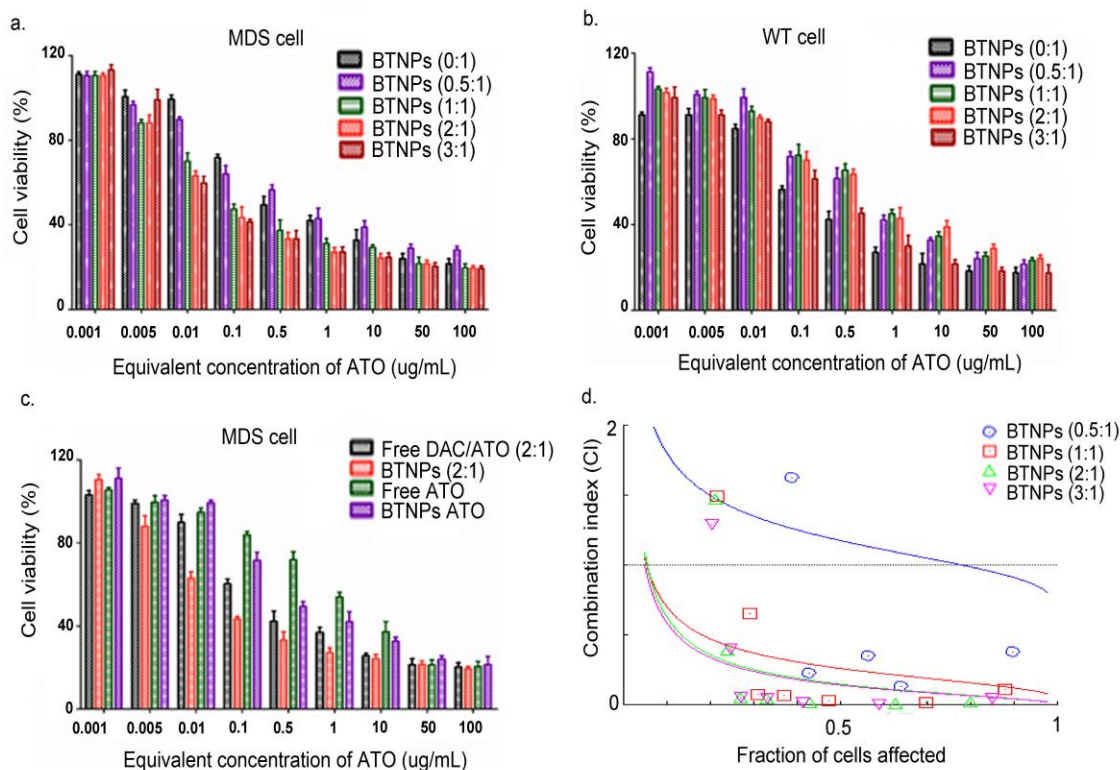


Fig.2. Cell growth inhibition and synergistic effects of BTNPs. a-c, Cell cytotoxicity were evaluated in MDS cells and WT cells. Data represent the mean \pm SEM (n=5). d, Synergistic inhibitory effects of BTNPs was calculated based on IC₅₀. Each CI score represents data from 7 different drug doses of single and paired-drug treatments with 5 biological replicates per condition.

3.3 BTNP-packaged DAC and ATO kills MDS cells by triggering cell apoptosis

Arsenic trioxide-induced apoptosis has been shown to result in therapeutic efficacy in MDS patients [38]. We compared apoptosis of MDS cells treated with drugs in their free form, in untargeted nanoparticles or in BTNP. While all three treatments caused cell apoptosis at with an equivalent concentration of ATO of 0.1 $\mu\text{g/mL}$, apoptotic cells were more than twice as many in samples treated with drugs packaged in nanoparticles than those with the same dosage of free drugs (Fig. 3a). Comparable cell killing by the targeted and untargeted nanoparticles was expected in the *in vitro* experiment, as bone niche targeting was not necessary for the

particle to reach the cells. Flow cytometer analysis corroborated effective cell killing by the packaged drug combination (Fig. 3b). Overall, these results further demonstrate the advantages of drug co-delivery over free drugs for MDS treatment.

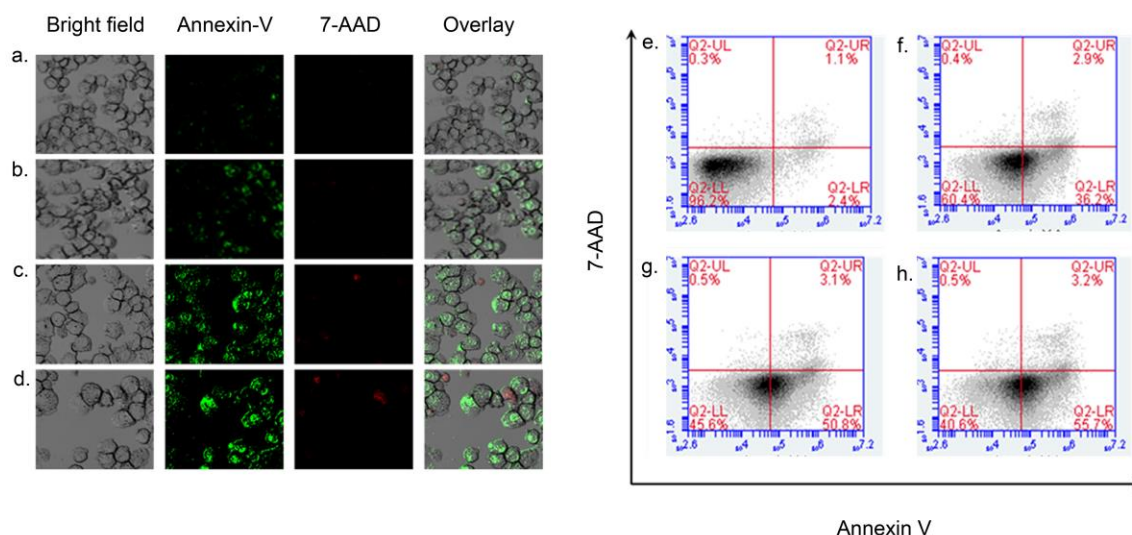


Fig.3. Apoptosis analysis of MDS cells induced by BTNPs. a, Representative CLSM images of apoptotic MDS cells after treatment with drugs at the concentration equivalent to ATO of 0.1 $\mu\text{g/mL}$. b-e, Flow cytometer analysis of apoptotic MDS cells treated with PBS, free drugs, untargeted NPs and BTNPs.

3.4 Pharmacokinetics and biodistribution studies of BTNPs

Pharmacokinetic analyses of ATO (Fig. 4a) and DAC (Fig. 4b) showed that BTNP delivery resulted in two to three orders of magnitude higher plasma drug concentration than the free drugs 12 h after injection. In addition, BTNPs showed sustained release of DAC and ATO for up to 72 hours. The area under curve (AUC_(0-∞)) of DAC in BTNP (2:1) was 4.5 times as high as free DAC, and that of ATO in BTNP (2:1) was 3.3 times over free ATO (Table 1). Biodistribution ATO and DAC from the free drugs, untargeted particles and BTNPs in MDS mice revealed that, although most nanoparticles accumulated in the liver 24h after intravenous injection, there were 6.7-fold 7.9-fold more DAC and ATO from BTNPs

accumulated in the femur than untargeted NPs, respectively (Fig. 4 c, d). No significant difference was observed on drug distribution in the other major organs including kidneys, spleen, lungs, and heart. These results indicate that BTNPs effectively targeted bone tissues and significantly enhanced drug accumulation in the bone marrow where the MDS cells locate.

Table 1. Pharmacokinetic parameters of DAC and ATO in different formulations.

Formulation [*]	AUC _(0-∞) ^a (h.mg/L)	t _{1/2} ^b (h)	CL ^c (L/h)
DAC in BTNPs (2:1)	8685.15	0.65	0.51
DAC in solution	1932.56	0.08	2.28
ATO in BTNPs (2:1)	4132.46	2.83	0.40
ATO in solution	1243.40	1.17	1.34

^{*} Average pharmacokinetic parameters values following single administration of each formulation (n=3).

^a AUC_(0-∞): The area under curve; ^b t_{1/2}: Elimination half-life; ^c CL: Clearance

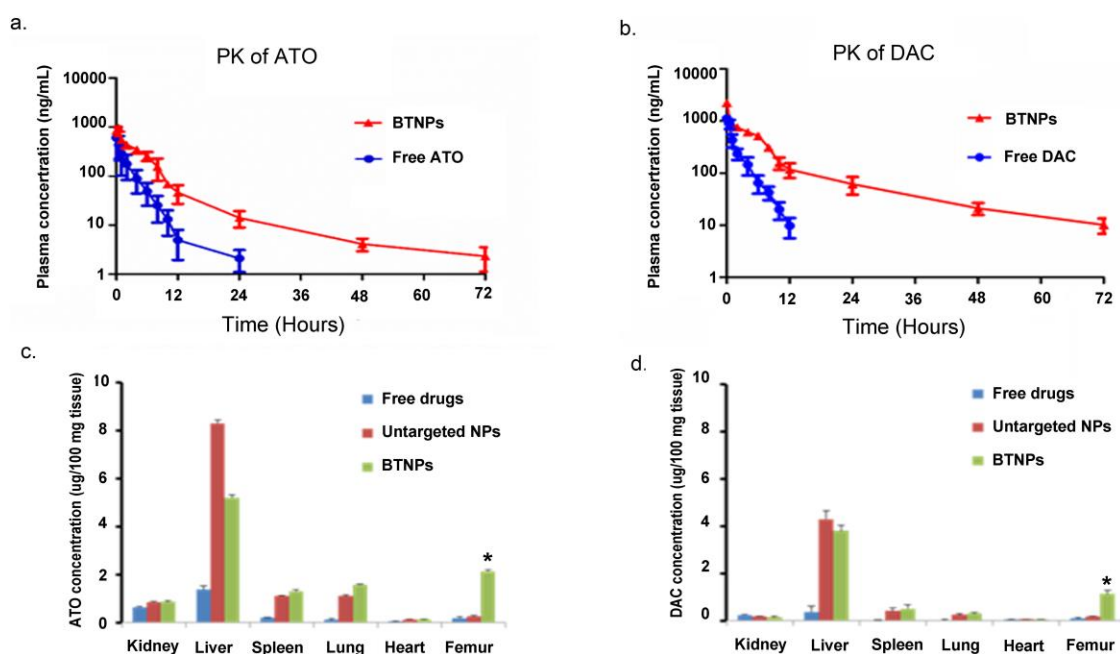


Fig.4. Pharmacokinetics and biodistribution studies of BTNPs. a-b, Pharmacokinetic profiles of BTNPs after one dose in MDS model mouse. Data represent the mean \pm SEM (n=4). c-d, Tissue

biodistribution of BTNPs in MDS mouse after 12 hour of administration. Data represent the mean \pm SEM (n=4).

3.5 Bone marrow enrichment of drug molecules provides therapeutic benefit in a murine model of MDS

The therapeutic goal for MDS is to achieve hematologic improvement and alteration of the disease's natural development. To evaluate efficacy of targeted nanoparticles in mice with MDS, CBC was measured weekly after treatment as indicator of hematologic improvement. Four weeks after BTNP treatment, WBC count increased in 62.5 % of the mice, and was restored to normal levels in 50% of the mice (Fig. 5a). In comparison, WBC count increased in only 31.3 % and 37.5 % of the mice treated with free drugs and untargeted particles, respectively, with only 25 % of mice displayed restored WBC count to normal levels in these groups. In the meanwhile, 56.2 % of BTNP treated mice had increased platelet counts, with 50 % of them displaying platelet counts in the normal range. In the free drug and untargeted particles treated groups, only 31.3 % and 37.5 % of the mice showed increased platelet counts, and 31.1 % of mice had platelet counts restored to normal range in these groups. (Fig. 5b). No increased in RBC counts was seen in the control group, while three mice presented further decreased RBC levels (Fig. 5c). Paired t-test analysis showed significant decrease of WBC, PLT and RBC in the PBS group after treatment, caused by MDS progression. On the contrary, in all drug treatment groups, CBCs were improved when compared with the PBS group. However, it should be noted that BTNPs treated mice showed significant increase in CBCs when compared to all the other treatments (free drugs and untargeted NPs). As a result, mice treated with BTNP showed significantly longer median survival than those treated with untargeted nanoparticles or free drugs (Fig. 5d). Interestingly, treatment with untargeted drug nanoparticles did not provide a significant survival benefit over the free drug combination, highlighting the

importance of bone marrow enrichment of the drug molecules through targeted drug delivery.

Analysis of blood smears provided further support for the therapeutic benefit from the treatment. Smears of peripheral blood from each group were analyzed to examine morphology of the hematopoietic cells (Smears of bone marrow cells did not show). Mice presented dysplastic cells in the PBS control group as indicated by black arrows (Fig. 5e). In treatment groups with DAC and ATO, myelodysplastic status got relieved. For the mice with favorable response, dysplastic cells disappeared and the number of platelets appeared to be obviously increased in PB smears especially in BTNPs target treatment group (Fig. 5h). It was kind of hard to find the platelets on PB smears of these mice due to thrombocytopenia (Fig. 5e-g). These results suggested that myelodysplastic syndrome could be best controlled in BTNPs target treatment group.

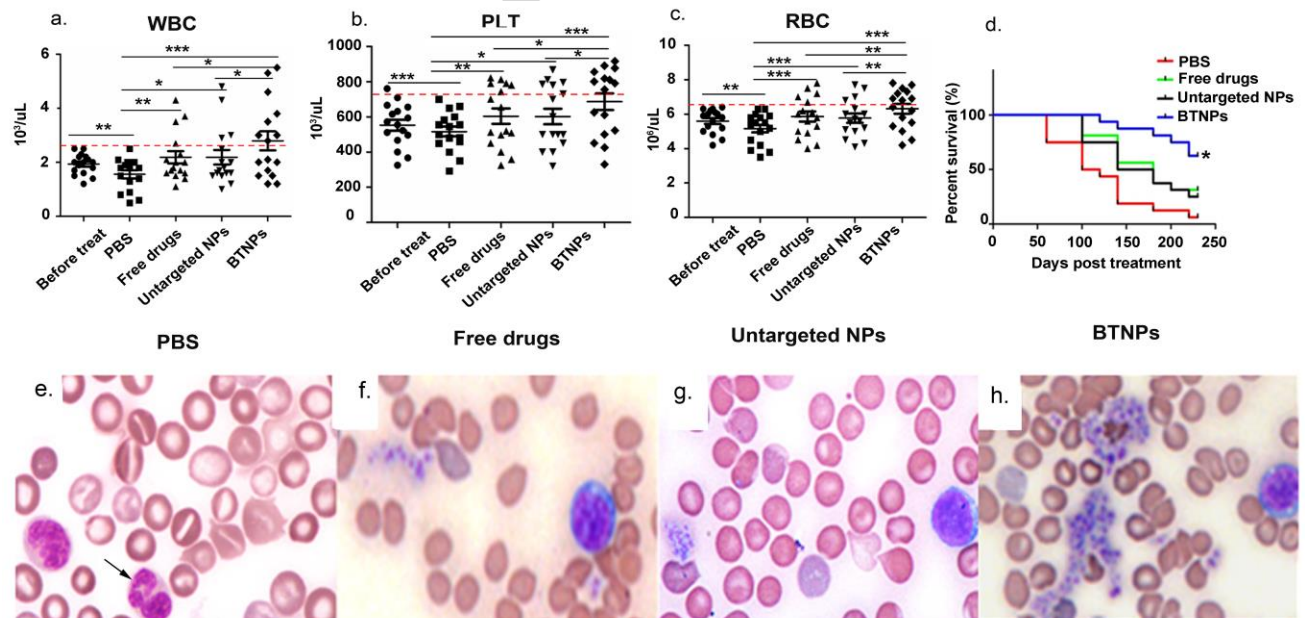


Fig.5. Therapeutic efficacy of BTNPs in MDS mouse model. a-c, Serial complete blood count measurements from MDS mice after treatment with DAC/ATO (Red line presents the threshold for normal WBC, PLT, and RBC count). Data represent the mean \pm SEM (n=16). d, Survival curves showing progression to death in different treated group of mice. Data collected from 3

separate experiments. e-h, Representative peripheral blood smears from MDS mice after treatment.

3.6 BNTP-delivered drugs inhibit DNMT1 and trigger apoptosis in bone marrow MDS cells

It has been previously reported that DAC is used to demethylate MDS through selective inhibition of DNA methyltransferase1 (DNMT1) [39]. We performed quantitative PCR analysis to analyze DNMT1 expression in bone marrow cells after treatment with BNTP-delivered drugs. DNMT1 mRNA levels in the free drug and untargeted NP treatment groups decreased by 43% comparing to the PBS control group; in comparison, DNMT1 mRNA dropped by 80% in the BNTP treatment group (Fig. 6a). This result showed that BNTP could more efficiently inhibit DNMT1 than untargeted NPs and free drugs. Cell cytotoxicity of decitabine was mainly mediated through DNA damage [40]. γ H2AX, a biomarker for DNA damage response, was measured by flow cytometric analysis to evaluate DNA damage after treatment with DAC (Fig. 6b). Intensity of fluorescence presented γ H2AX expressing level. MDS bone marrow cell treated with BNTPs had the lowest level of γ H2AX. This suggests that DNA of MDS bone marrow cell was protected more efficiently upon treatment with BNTPs. These results suggest that BNTPs enhanced demethylation function of DAC to improve therapy efficacy on MDS and reduced DNA damage by DAC when compared to untargeted NPs and free drugs.

Flow cytometer was also performed to determine bone marrow cell apoptosis after treatment with BNTPs. Apoptosis rates in free drug and untargeted NPs treatment groups increased by 3.5-4.2 folds comparing to the PBS group, and BNTP treatment further induced apoptosis (Fig. 6c). Thus, targeted delivery of ATO through BNTP could enhance apoptotic effects of ATO on bone marrow cells. As

indicated by the yellow arrows in (Fig. 6d-g), obvious cell apoptosis can be seen in the livers of groups treated with free ATO and untargeted nanoparticles, while comparable levels of apoptotic cell were found in the control group (PBS) and BTNPs treated groups. These data show that BTNPs could significantly reduce hepatotoxicity caused by non-specific action of ATO.

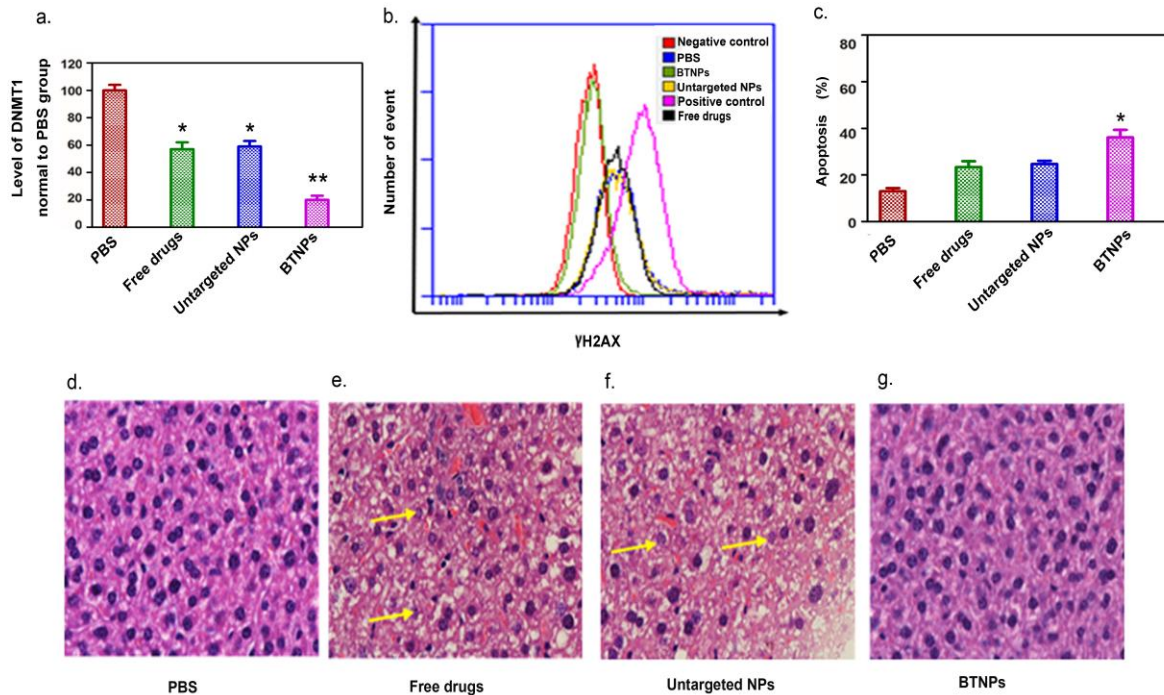


Fig.6. Inhibition of DNMT1 and apoptosis of MDS bone marrow cells (BM cells) after treatment with BTNPs. a. RT-PCR analysis of DNMT1 mRNA level in BM cells. b, Flow cytometer analysis of γ H2AX expression in BM cells. c, Apoptosis percentage of BM cells after treatment. Data represent the mean \pm SEM (n=5); d-g. Representative H&E staining show apoptotic liver cell from MDS mouse after treatment.

4. Discussion

Clinical use of many chemotherapy drugs is currently limited by the potential toxic effect on both tumor and healthy cells [41]. In fact, it is still a challenge to develop efficient and safe delivery systems capable of targeted delivery of chemotherapy drugs to the tumor site. A selective increase of drug concentration in the bone

marrow is required to reduce systemic toxicity and increase efficacy in the treatment of MDS and other bone marrow related malignant tumors. Nanoparticles so far developed for targeting bone marrow include two major classes: liposomal-based and polymeric-based bone targeting [42]. Both these approaches present specific advantages for drug delivery. However, they both also exhibit limitations that significantly hinder clinical application. To combine the unique advantage of both polymeric nanoparticles and liposomes, and overcome their specific drawbacks, we developed a new class of bone-targeting nanoparticles, BTNPs, for the co-delivery of ATO and DAC. BTNPs developed in this work exhibit high drug loading efficiency, sustained-release profiles, good colloidal stability, specific bone-targeting ability and uniform size distribution. In our study, BTNPs composition for therapeutic efficacy studies was selected to be 20% lipid and 80% polymer to obtain a size in the 10 nm – 100 nm range, optimal for endocytosis uptake in tumor cells[43]. In addition, BTNPs display good colloidal stability due to the presence of PEG on the surface, which prevents protein adsorption and aggregation of nanoparticles. This property presents significant additional advantage of BTNPs over polymeric particles since polymeric particles have been reported to easily aggregate in serum due to their hydrophobic surface [25]. We demonstrated that our BTNPs have an 87.5% ATO loading efficiency, whereas previous studies report only a 26.3% loading efficiency by liposomal formulation [44]. We also demonstrated a sustained release of ATO from BTNPs over 72 hours, while a previous study reported more than 60% ATO being released within only 3 hours from a liposomal formulation [44]. Similar results were observed in another study on DAC release from liposomes, where more than 90% DAC was released within the first 24 hours [45]. On the contrary, BTNPs exhibit sustained-release of DAC three times longer when compared to liposomal formulations. Overall, BTNPs inherit high loading efficiency and sustained release profile from polymeric nanoparticles and exhibit good colloidal stability benefiting from PEG-lipid layer.

With our study, we demonstrated that BTNPs co-encapsulation also enhances synergistic effect of ATO and DAC on MDS cells. DAC is known to have potential demethylation effects on MDS cells, but no growth inhibition effect at low concentrations [46, 47]. On the contrary, ATO has been reported to reduce MDS cell viability by inducing apoptosis [48]. Our results not only confirm these

findings, but also demonstrate complete synergistic effect of DAC and ATO in BTNPs formulations containing higher DAC/ATO ratios (1:1 to 3:1). It should be noted that a synergistic effect was also observed in the free mixture of DAC/ATO (2:1) when compared to DAC and ATO alone. However, the IC₅₀ of the free mixture DAC/ATO (2:1) was still much higher than that of BTNPs (2:1). Thus, BTNP formulation (2:1) further increased the synergistic effects of DAC and ATO on MDS cells compared to the free mixture DAC/ATO (2:1). This benefit is likely owed to intrinsic advantages of nanoparticle-based delivery over the free form, namely enhanced cell uptake (Fig 3 b-d) and sustained drug release. Unexpectedly, BTNPs (0.5:1) shows higher IC₅₀ than BTNPs ATO, which suggests a possible antagonistic effect of BTNPs (0.5:1) at low fraction of affected cells, and synergistic effect at high fraction of affected cells. This type of contradicting behavior of two drugs at different ratio has been previously reported for others combinatorial drugs [49].

Our plasma concentration studies of BTNPs-treated MDS mice showed sustained release of drugs from BTNPs *in vivo*, confirming our *in vitro* results. As expected, BTNPs and untargeted NPs showed no significant difference in targeting MDS bone marrow cell apoptosis *in vitro*, while BTNPs significantly enhanced accumulation of nanoparticles in the bone marrow niche of MDS mice. Tissue distribution analysis showed that BTNPs enabled increase accumulation of DAC and ATO in the bone marrow up to 6.7-fold and 7.9-fold, respectively. In previous literature, the *in vivo* biodistribution of alendronate conjugated polymer (PTX-PEG-ALN, DOX-hyd-PEG-ALN) micelles for bone targeted delivery of paclitaxel and doxorubicin increased only around 3 and 4 fold accumulation of drugs in bone, respectively [22, 23]. The more efficient bone targeting of BTNPs with respect to alendronate conjugated polymeric micelles can be attributed to enhanced bone marrow absorption and reduced burst release profile of BTNPs. The lipid layer surrounding BTNPs facilitates uptake by MDS cells due to its cell compatibility. More importantly, the lipid layer enhances drug retention in BTNPs during the initial release phase [25]. This will maximally increase drug accumulation in targeted tissues during BTNP-delivery. The *in vivo* biodistribution of alendronate-conjugated liposomes (LIP-ALN) has not been investigated, but a comparison can be performed based on loading efficiency. BTNPs' loading efficiency is significantly higher when compared to alendronate-conjugated liposomes (89% for

BTNPs vs 34%-50% for LIP-ALN) [24]. This advantage of BTNPs likely results from their polymeric core.

In our study we evaluated therapeutic efficacy by monitoring WBC and PLT, two important indexes for diagnosis of MDS in clinic. BTNPs significantly increased percentages of recovered WBC and PLT in MDS mice compared to free drugs and untargeted NPs. Notably, the sustained release advantage of untargeted NPs was not sufficient to result in significant changes in CBC and survival time when compared to free drugs. This stresses the importance of bone marrow targeting to reach sufficient levels of drug accumulation in bone marrow. These results could additionally explain why no single patient has shown complete remission in a recent phase I clinical study on MDS treatment with combination of free DAC and ATO (three stable disease; two progressions) [5]. Therefore, our promising results in mice suggest that targeted delivery to bone marrow through BTNPs could greatly improve outcome for MDS patients in clinic. BNTP co-delivery of DAC and ATO not only improved therapeutic efficacy, but also reduced systemic toxicity by increasing drug accumulation in the bone marrow of MDS mice. Decitabine treatment of MDS has been reported to have cytotoxic effects on bone marrow cells, requiring pulse-cycled administration to minimize cytotoxicity and increase DNMT1 depletion [44]. Compared to the combination of free drugs and untargeted NPs, BTNPs result in greater DNMT1 depletion, without increasing DNA damage to healthy bone marrow cells. This is likely a benefit due to sustained release and bone targeting properties of BTNPs, which ensures a high enough DAC concentration for effective DNMT1 depletion, but no cell toxicity to bone marrow cells. Hepatotoxicity through liver cell apoptosis is instead the main systemic toxicity caused by arsenic trioxide [50]. However, a significant reduction of apoptotic liver cells was seen in BTNPs treated MDS mice as a result of the bone targeting ability of BTNPs. Overall, our data support further clinical translation of BTNPs to improve current outcome of MDS with low systemic toxicity in clinic.

5. Conclusions

In this study, DAC and ATO were co-delivered in a bone-targeting polymeric/lipid nanoparticle formulation (BNTP) for MDS treatment, and resulted in a dual-acting

synergistic mechanism. Our *in vitro* studies suggested that BTNPs (DAC: ATO =2:1) exhibited synergistic enhancement of MDS cell growth inhibition, while reducing cell toxicity in WT cells. Thanks to their targeting ability, BTNPs showed a great advantage also in the *in vivo* treatment of an MDS mouse model with respect to free drugs and delivery via untargeted nanoparticles. BTNPs also significantly reduced hepatotoxicity, the main adverse effect of ATO in clinic. In conclusion, using BTNPs to co-deliver DAC and ATO, not only generated synergistic effect in the treatment of MDS cells in a mouse model, but also reduced systemic toxicity. These studies suggest that BTNPs could provide an efficient combinatorial strategy for bone-targeted treatment of MDS in the clinic.

Acknowledgement

The authors acknowledge financial support from the National Institute of Health grant 1R01CA193880-01A1, and U54CA210181 (MF), U.S. Department of Defense grant W81XWH-12-1-0414 (MF), the Ernest Cockrell Jr. Distinguished Endowed Chair fund (MF), and Dottie and Jimmy C. Adair Myelodysplastic Syndrome Treatment and Research Funding.

Reference

- [1] L. Ades, R. Itzykson, P. Fenaux, Myelodysplastic syndromes, *Lancet*, 383 (2014) 2239-2252.
- [2] B.D. Cheson, P.L. Greenberg, J.M. Bennett, B. Lowenberg, P.W. Wijermans, S.D. Nimer, A. Pinto, M. Beran, T.M. de Witte, R.M. Stone, M. Mittelman, G.F. Sanz, S.D. Gore, C.A. Schiffer, H. Kantarjian, Clinical application and proposal for modification of the International Working Group (IWG) response criteria in myelodysplasia, *Blood*, 108 (2006) 419-425.
- [3] Y. Jiang, A. Dunbar, L.P. Gondek, S. Mohan, M. Rataul, C. O'Keefe, M. Sekeres, Y. Sauntharajah, J.P. Maciejewski, Aberrant DNA methylation is a dominant mechanism in MDS progression to AML, *Blood*, 113 (2009) 1315-1325.
- [4] R. Bejar, D.P. Steensma, Recent developments in myelodysplastic syndromes, *Blood*, 124 (2014) 2793-2803.
- [5] J.S. Welch, J.M. Kilo, F. Gao, E. Procknow, G.L. Uy, K.E. Stockerl-Goldstein, C.N. Abboud, P. Westervelt, J.F. DiPersio, A. Hassan, A.F. Cashen, R. Vij, Combination decitabine, arsenic trioxide, and ascorbic acid for the treatment of myelodysplastic syndrome and acute myeloid leukemia: a phase I study, *Am J Hematol*, 86 (2011) 796-800.

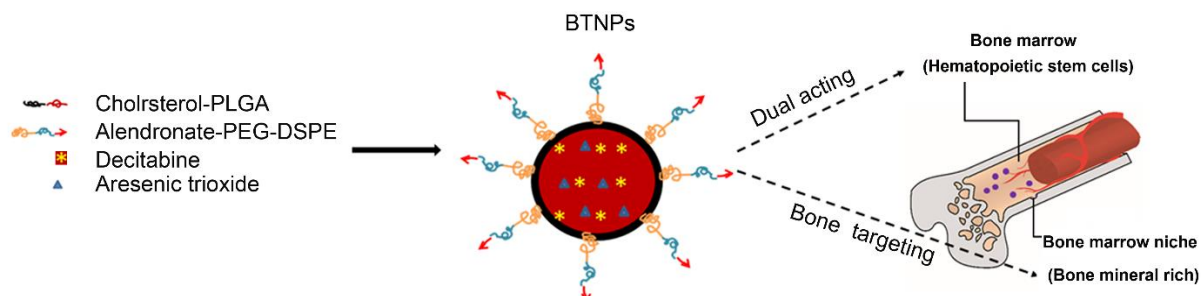
- [6] H. Kantarjian, J.P. Issa, C.S. Rosenfeld, J.M. Bennett, M. Albitar, J. DiPersio, V. Klimek, J. Slack, C. de Castro, F. Ravandi, R. Helmer, 3rd, L. Shen, S.D. Nimer, R. Leavitt, A. Raza, H. Saba, Decitabine improves patient outcomes in myelodysplastic syndromes: results of a phase III randomized study, *Cancer*, 106 (2006) 1794-1803.
- [7] C. Niu, H. Yan, T. Yu, H.P. Sun, J.X. Liu, X.S. Li, W. Wu, F.Q. Zhang, Y. Chen, L. Zhou, J.M. Li, X.Y. Zeng, R.R. Yang, M.M. Yuan, M.Y. Ren, F.Y. Gu, Q. Cao, B.W. Gu, X.Y. Su, G.Q. Chen, S.M. Xiong, T.D. Zhang, S. Waxman, Z.Y. Wang, Z. Chen, J. Hu, Z.X. Shen, S.J. Chen, Studies on treatment of acute promyelocytic leukemia with arsenic trioxide: remission induction, follow-up, and molecular monitoring in 11 newly diagnosed and 47 relapsed acute promyelocytic leukemia patients, *Blood*, 94 (1999) 3315-3324.
- [8] G. Chen, Y. Wang, H. Huang, F. Lin, D. Wu, A. Sun, H. Chang, Y. Feng, Combination of DNA methylation inhibitor 5-azacytidine and arsenic trioxide has synergistic activity in myeloma, *Eur J Haematol*, 82 (2009) 176-183.
- [9] S. Li, Y. Ding, Q. Niu, S. Xu, L. Pang, R. Ma, M. Jing, G. Feng, J.X. Tang, Q. Zhang, X. Ma, Y. Yan, J. Zhang, M. Wei, H.X. Wang, F. Li, S. Guo, Lutein has a protective effect on hepatotoxicity induced by arsenic via Nrf2 signaling, *Biomed Res Int*, 2015 (2015) 315205.
- [10] H.J. Iland, K. Bradstock, S.G. Supple, A. Catalano, M. Collins, M. Hertzberg, P. Browett, A. Grigg, F. Firkin, A. Hugman, J. Reynolds, J. Di Iulio, C. Tiley, K. Taylor, R. Filshie, M. Seldon, J. Taper, J. Szer, J. Moore, J. Bashford, J.F. Seymour, All-trans-retinoic acid, idarubicin, and IV arsenic trioxide as initial therapy in acute promyelocytic leukemia (APML4), *Blood*, 120 (2012) 1570-1580; quiz 1752.
- [11] A. Eden, F. Gaudet, A. Waghmare, R. Jaenisch, Chromosomal instability and tumors promoted by DNA hypomethylation, *Science*, 300 (2003) 455.
- [12] H. Wu, Y. Chen, J. Liang, B. Shi, G. Wu, Y. Zhang, D. Wang, R. Li, X. Yi, H. Zhang, L. Sun, Y. Shang, Hypomethylation-linked activation of PAX2 mediates tamoxifen-stimulated endometrial carcinogenesis, *Nature*, 438 (2005) 981-987.
- [13] H. Wang, J. Yu, X. Lu, X. He, Nanoparticle systems reduce systemic toxicity in cancer treatment, *Nanomedicine (Lond)*, 11 (2016) 103-106.
- [14] C. Poon, C. He, D. Liu, K. Lu, W. Lin, Self-assembled nanoscale coordination polymers carrying oxaliplatin and gemcitabine for synergistic combination therapy of pancreatic cancer, *J Control Release*, 201 (2015) 90-99.
- [15] X. Zhang, L. Li, C. Li, H. Zheng, H. Song, F. Xiong, T. Qiu, J. Yang, Cisplatin-crosslinked glutathione-sensitive micelles loaded with doxorubicin for combination and targeted therapy of tumors, *Carbohydr Polym*, 155 (2017) 407-415.
- [16] S. Zalba, A.M. Contreras, A. Haeri, T.L. Ten Hagen, I. Navarro, G. Koning, M.J. Garrido, Cetuximab-oxaliplatin-liposomes for epidermal growth factor receptor targeted chemotherapy of colorectal cancer, *J Control Release*, 210 (2015) 26-38.
- [17] J.L. Vivero-Escoto, M. Elnagheeb, Mesoporous Silica Nanoparticles Loaded with Cisplatin and Phthalocyanine for Combination Chemotherapy and Photodynamic Therapy in vitro, *Nanomaterials (Basel)*, 5 (2015) 2302-2316.
- [18] L. Zhao, L. Zhu, F. Liu, C. Liu, D. Shan, Q. Wang, C. Zhang, J. Li, J. Liu, X. Qu, Z. Yang, pH triggered injectable amphiphilic hydrogel containing doxorubicin and paclitaxel, *Int J Pharm*, 410 (2011) 83-91.
- [19] G. Xia, B. Chen, J. Ding, C. Gao, H. Lu, Z. Shao, F. Gao, X. Wang, Effect of magnetic Fe₃O₄ nanoparticles with 2-methoxyestradiol on the cell-cycle progression and apoptosis of myelodysplastic syndrome cells, *Int J Nanomedicine*, 6 (2011) 1921-1927.
- [20] S. Ashton, Y.H. Song, J. Nolan, E. Cadogan, J. Murray, R. Odedra, J. Foster, P.A. Hall, S. Low, P. Taylor, R. Ellston, U.M. Polanska, J. Wilson, C. Howes, A. Smith, R.J. Goodwin, J.G. Swales, N. Strittmatter, Z. Takats, A. Nilsson, P. Andren, D. Trueman, M. Walker, C.L. Reimer, G. Troiano, D. Parsons, D. De Witt, M. Ashford, J. Hrkach, S. Zale, P.J. Jewsbury, S.T. Barry, Aurora kinase inhibitor nanoparticles target tumors with favorable therapeutic index in vivo, *Sci Transl Med*, 8 (2016) 325ra317.

- [21] A. Swami, M.R. Reagan, P. Basto, Y. Mishima, N. Kamaly, S. Glavey, S. Zhang, M. Moschetta, D. Seevaratnam, Y. Zhang, J. Liu, M. Memarzadeh, J. Wu, S. Manier, J. Shi, N. Bertrand, Z.N. Lu, K. Nagano, R. Baron, A. Sacco, A.M. Roccaro, O.C. Farokhzad, I.M. Ghobrial, Engineered nanomedicine for myeloma and bone microenvironment targeting, *Proc Natl Acad Sci U S A*, 111 (2014) 10287-10292.
- [22] K. Miller, C. Clementi, D. Polyak, A. Eldar-Boock, L. Benayoun, I. Barshack, Y. Shaked, G. Pasut, R. Satchi-Fainaro, Poly(ethylene glycol)-paclitaxel-alendronate self-assembled micelles for the targeted treatment of breast cancer bone metastases, *Biomaterials*, 34 (2013) 3795-3806.
- [23] W.L. Ye, Y.P. Zhao, H.Q. Li, R. Na, F. Li, Q.B. Mei, M.G. Zhao, S.Y. Zhou, Doxorubicin-poly(ethylene glycol)-alendronate self-assembled micelles for targeted therapy of bone metastatic cancer, *Sci Rep*, 5 (2015) 14614.
- [24] M.B. (2011), Bone marrow targeted liposomal drug delivery systems, (Doctoral dissertation) Retrieved from <http://citeseerx.ist.psu.edu/viewdoc/download?doi=10.1.1.470.2038&rep=rep1&type=pdf>.
- [25] L. Zhang, J.M. Chan, F.X. Gu, J.W. Rhee, A.Z. Wang, A.F. Radovic-Moreno, F. Alexis, R. Langer, O.C. Farokhzad, Self-assembled lipid-polymer hybrid nanoparticles: a robust drug delivery platform, *ACS Nano*, 2 (2008) 1696-1702.
- [26] B. Mandal, H. Bhattacharjee, N. Mittal, H. Sah, P. Balabathula, L.A. Thoma, G.C. Wood, Core-shell-type lipid-polymer hybrid nanoparticles as a drug delivery platform, *Nanomedicine*, 9 (2013) 474-491.
- [27] K. Hadinoto, A. Sundaresan, W.S. Cheow, Lipid-polymer hybrid nanoparticles as a new generation therapeutic delivery platform: a review, *Eur J Pharm Biopharm*, 85 (2013) 427-443.
- [28] T.R. Fadel, F.A. Sharp, N. Vudattu, R. Ragheb, J. Garyu, D. Kim, E. Hong, N. Li, G.L. Haller, L.D. Pfefferle, S. Justesen, K.C. Herold, T.M. Fahmy, A carbon nanotube-polymer composite for T-cell therapy, *Nat Nanotechnol*, 9 (2014) 639-647.
- [29] M.A. Dobrovolskaia, A.K. Patri, J. Zheng, J.D. Clogston, N. Ayub, P. Aggarwal, B.W. Neun, J.B. Hall, S.E. McNeil, Interaction of colloidal gold nanoparticles with human blood: effects on particle size and analysis of plasma protein binding profiles, *Nanomedicine*, 5 (2009) 106-117.
- [30] D. Liu, C. Poon, K. Lu, C. He, W. Lin, Self-assembled nanoscale coordination polymers with trigger release properties for effective anticancer therapy, *Nat Commun*, 5 (2014) 4182.
- [31] Y. Zhang, J. Sun, Y. Gao, Y. Kong, Y. Xu, W. Jia, C. Liao, P. Zhang, H. Lian, X. Han, D. Li, Y. Geng, Z. He, An HPLC-MS/MS method for simultaneous determination of decitabine and its valyl prodrug valdecitabine in rat plasma, *J Chromatogr B Analyt Technol Biomed Life Sci*, 917-918 (2013) 78-83.
- [32] Y. Fukai, M. Hirata, M. Ueno, N. Ichikawa, H. Kobayashi, H. Saitoh, T. Sakurai, K. Kinoshita, T. Kaise, S. Ohta, Clinical pharmacokinetic study of arsenic trioxide in an acute promyelocytic leukemia (APL) patient: speciation of arsenic metabolites in serum and urine, *Biol Pharm Bull*, 29 (2006) 1022-1027.
- [33] R.W. Ahn, F. Chen, H. Chen, S.T. Stern, J.D. Clogston, A.K. Patri, M.R. Raja, E.P. Swindell, V. Parimi, V.L. Cryns, T.V. O'Halloran, A novel nanoparticulate formulation of arsenic trioxide with enhanced therapeutic efficacy in a murine model of breast cancer, *Clin Cancer Res*, 16 (2010) 3607-3617.
- [34] Y. Tomikoshi, M. Nomura, N. Okudaira, H. Sakagami, H. Wakabayashi, Enhancement of Cytotoxicity of Three Apoptosis-inducing Agents Against Human Oral Squamous Cell Carcinoma Cell Line by Benzoxazinotropone, *In Vivo*, 30 (2016) 645-650.
- [35] M. Karahoca, R.L. Momparler, Pharmacokinetic and pharmacodynamic analysis of 5-aza-2'-deoxycytidine (decitabine) in the design of its dose-schedule for cancer therapy, *Clin Epigenetics*, 5 (2013) 3.
- [36] H. Pan, M. Sima, P. Kopeckova, K. Wu, S. Gao, J. Liu, D. Wang, S.C. Miller, J. Kopecek, Biodistribution and pharmacokinetic studies of bone-targeting N-(2-hydroxypropyl)methacrylamide copolymer-alendronate conjugates, *Mol Pharm*, 5 (2008) 548-558.
- [37] S.W. Choi, J.H. Kim, Design of surface-modified poly(D,L-lactide-co-glycolide) nanoparticles for targeted drug delivery to bone, *J Control Release*, 122 (2007) 24-30.

- [38] D.M. Kerbaui, V. Lesnikov, N. Abbasi, S. Seal, B. Scott, H.J. Deeg, NF-kappaB and FLIP in arsenic trioxide (ATO)-induced apoptosis in myelodysplastic syndromes (MDSs), *Blood*, 106 (2005) 3917-3925.
- [39] K. Ghoshal, J. Datta, S. Majumder, S. Bai, H. Kutay, T. Motiwala, S.T. Jacob, 5-Aza-deoxycytidine induces selective degradation of DNA methyltransferase 1 by a proteasomal pathway that requires the KEN box, bromo-adjacent homology domain, and nuclear localization signal, *Mol Cell Biol*, 25 (2005) 4727-4741.
- [40] K. Maes, E. De Smedt, M. Lemaire, H. De Raeve, E. Menu, E. Van Valckenborgh, S. McClue, K. Vanderkerken, E. De Bruyne, The role of DNA damage and repair in decitabine-mediated apoptosis in multiple myeloma, *Oncotarget*, 5 (2014) 3115-3129.
- [41] A.K. Mitra, V. Agrahari, A. Mandal, K. Cholkar, C. Natarajan, S. Shah, M. Joseph, H.M. Trinh, R. Vaishya, X. Yang, Y. Hao, V. Khurana, D. Pal, Novel delivery approaches for cancer therapeutics, *J Control Release*, 219 (2015) 248-268.
- [42] W. Gu, C. Wu, J. Chen, Y. Xiao, Nanotechnology in the targeted drug delivery for bone diseases and bone regeneration, *Int J Nanomedicine*, 8 (2013) 2305-2317.
- [43] M. Goldberg, R. Langer, X. Jia, Nanostructured materials for applications in drug delivery and tissue engineering, *J Biomater Sci Polym Ed*, 18 (2007) 241-268.
- [44] P. Kallinteri, D. Fatouros, P. Klepetsanis, S.G. Antimisari, Arsenic trioxide liposomes: encapsulation efficiency and in vitro stability, *J Liposome Res*, 14 (2004) 27-38.
- [45] M.P.V.V.B.N.R.S.I. Begum, Preparation and evaluation of decitabine liposomes, *Indo American Journal of Pharmaceutical Sciences*, 2 (2015) 1264-1273.
- [46] H.I. Saba, Decitabine in the treatment of myelodysplastic syndromes, *Ther Clin Risk Manag*, 3 (2007) 807-817.
- [47] M. Fuller, M. Klein, E. Schmidt, C. Rohde, S. Gollner, I. Schulze, J. Qianli, W.E. Berdel, B. Edemir, C. Muller-Tidow, P. Tschanter, 5-azacytidine enhances efficacy of multiple chemotherapy drugs in AML and lung cancer with modulation of CpG methylation, *Int J Oncol*, 46 (2015) 1192-1204.
- [48] X. Cai, Y.L. Shen, Q. Zhu, P.M. Jia, Y. Yu, L. Zhou, Y. Huang, J.W. Zhang, S.M. Xiong, S.J. Chen, Z.Y. Wang, Z. Chen, G.Q. Chen, Arsenic trioxide-induced apoptosis and differentiation are associated respectively with mitochondrial transmembrane potential collapse and retinoic acid signaling pathways in acute promyelocytic leukemia, *Leukemia*, 14 (2000) 262-270.
- [49] R.H. Shanks, D.A. Rizzieri, J.L. Flowers, O.M. Colvin, D.J. Adams, Preclinical evaluation of gemcitabine combination regimens for application in acute myeloid leukemia, *Clin Cancer Res*, 11 (2005) 4225-4233.
- [50] A.P. Singh, R.K. Goel, T. Kaur, Mechanisms pertaining to arsenic toxicity, *Toxicol Int*, 18 (2011) 87-93.

Table 1. Pharmacokinetic parameters of DAC and ATO in different formulations.

Formulation [*]	AUC _(0-∞) ^a (h.mg/L)	t _{1/2} ^b (h)	CL ^c (L/h)
DAC in BTNPs (2:1)	8685.15	0.65	0.51
DAC in solution	1932.56	0.08	2.28
ATO in BTNPs (2:1)	4132.46	2.83	0.40
ATO in solution	1243.40	1.17	1.34



Graphical abstract